Measurements of double-helicity asymmetries in inclusive J/ψ production in longitudinally polarized p+p collisions at √s = 510 GeV

(PHENIX Collaboration) Adare, A.; ...; Makek, Mihael; ...; Zou, L.

Measurements of double-helicity asymmetries in inclusive J/ψ production in longitudinally polarized $p+p$ collisions at $\sqrt{s}=510$ GeV

A. Adare,[13] C. Aidala,[41] N. N. Ajitanand,[58] Y. Akiba,[53,54,†] R. Akimoto,[12] M. Alfred,[22] N. Apadula,[27,59] Y. Aramaki,[53] H. Asano,[34,53] E. T. Atomssa,[59] T. C. Awes,[49] B. Azmoun,[7] V. Babintsev,[23] M. Bai,[6] N. S. Bandara,[40] B. Bannier,[59] K. N. Barish,[8] S. Bathe,[5,54] A. Bazilevsky,[7] M. Beaumier,[8] S. Beckman,[13] R. Belmont,[13,41] A. Berdnikov,[56] Y. Berdnikov,[56] D. Black,[8] D. S. Blau,[33] J. S. Bok,[47] K. Boyle,[54] M. L. Brooks,[37] J. Bryslawskyj,[5,8] H. Buesching,[7] V. Bumazhnov,[23] S. Campbell,[14,27] C.-H. Chen,[54] C. Y. Chi,[14] M. Chiu,[7] I. J. Choi,[24] J. B. Choi,[10,*] T. Chujo,[62] Z. Citron,[64] M. Csanád,[16] T. Csörgő,[65] T. W. Danley,[48] A. Datta,[46] M. S. Daugherity,[1] G. David,[7] K. DeBlasio,[46] K. Dehmelt,[59] A. Denisov,[23] A. Deshpande,[54,59] E. J. Desmond,[7] L. Ding,[27] A. Dion,[59] P. B. Diss,[39] J. H. Do,[66] A. Drees,[59] K. A. Drees,[6] J. M. Durham,[37] A. Durum,[23] A. Enokizono,[53,55] H. En'yo,[53] S. Esumi,[62] B. Fadem,[42] N. Feege,[59] D. E. Fields,[46] M. Finger,[9] M. Finger, Jr.,[9] S. L. Fokin,[33] J. E. Frantz,[48] A. Franz,[7] A. D. Frawley,[18] C. Gal,[59] P. Gallus,[15] P. Garg,[3,59] H. Ge,[59] F. Giordano,[24] A. Glenn,[36] Y. Goto,[53,54] N. Grau,[2] S. V. Greene,[63] M. Grosse Perdekamp,[24] Y. Gu,[58] T. Gunji,[12] H. Guragain,[19] T. Hachiya,[53,54] J. S. Haggerty,[7] K. I. Hahn,[17] H. Hamagaki,[12] H. F. Hamilton,[1] S. Y. Han,[17] J. Hanks,[59] S. Hasegawa,[28] T. O. S. Haseler,[19] K. Hashimoto,[53,55] X. He,[19] T. K. Hemmick,[59] J. C. Hill,[27] R. S. Hollis,[8] K. Homma,[21] B. Hong,[32] T. Hoshino,[21] N. Hotvedt,[27] J. Huang,[7,37] S. Huang,[63] Y. Ikeda,[53] K. Imai,[28] Y. Imazu,[53] M. Inaba,[62] A. Iordanova,[8] D. Isenhower,[1] D. Ivanishchev,[52] B. V. Jacak,[59] S. J. Jeon,[43] M. Jezghani,[19] J. Jia,[7,58] X. Jiang,[37] B. M. Johnson,[7,19] E. Joo,[32] K. S. Joo,[43] D. Jouan,[50] D. S. Jumper,[24] S. Kanda,[12,31,53] J. H. Kang,[66] J. S. Kang,[20] D. Kawall,[40] A. V. Kazantsev,[33] J. A. Key,[46] V. Khachatryan,[59] A. Khanzadeev,[52] K. Kihara,[62] C. Kim,[32] D. H. Kim,[17] D. J. Kim,[29] E.-J. Kim,[10] G. W. Kim,[17] H.-J. Kim,[66] M. Kim,[57] Y. K. Kim,[20] B. Kimelman,[42] E. Kistenev,[7] R. Kitamura,[12] J. Klatsky,[18] D. Kleinjan,[8] P. Kline,[59] T. Koblesky,[13] M. Kofarago,[16,65] B. Komkov,[52] J. Koster,[54] D. Kotov,[52,56] K. Kurita,[55] M. Kurosawa,[53,54] Y. Kwon,[66] R. Lacey,[58] J. G. Lajoie,[27] A. Lebedev,[27] K. B. Lee,[37] S. Lee,[66] S. H. Lee,[59] M. J. Leitch,[37] M. Leitgab,[24] X. Li,[11] S. H. Lim,[66] M. X. Liu,[37] D. Lynch,[7] Y. I. Makdisi,[6] M. Makek,[64,67] A. Manion,[59] V. I. Manko,[33] E. Mannel,[7] M. McCumber,[37] P. L. McGaughey,[37] D. McGlinchey,[13] C. McKinney,[24] A. Meles,[47] M. Mendoza,[8] B. Meredith,[14] Y. Miake,[62] A. C. Mignerey,[39] A. J. Miller,[1] A. Milov,[64] D. K. Mishra,[4] J. T. Mitchell,[7] S. Miyasaka,[53,61] S. Mizuno,[53,62] A. K. Mohanty,[4] P. Montuenga,[24] T. Moon,[66] D. P. Morrison,[7] T. V. Moukhanova,[33] T. Murakami,[34,53] J. Murata,[53,55] A. Mwai,[58] S. Nagamiya,[31,53] K. Nagashima,[21] J. L. Nagle,[13] M. I. Nagy,[16] I. Nakagawa,[53,54] H. Nakagomi,[53,62] K. Nakano,[53,61] C. Nattrass,[60] P. K. Netrakanti,[4] M. Nihashi,[21,53] T. Niida,[62] S. Nishimura,[12,31] R. Nouicer,[7,54] T. Novák,[30,65] N. Novitzky,[29,59] A. S. Nyanin,[33] E. O'Brien,[7] C. A. Ogilvie,[27] J. D. Orjuela Koop,[13] J. D. Osborn,[41] A. Oskarsson,[38] K. Ozawa,[31] R. Pak,[7] V. Pantuev,[25] V. Papavassiliou,[47] J. S. Park,[57] S. Park,[57] S. F. Pate,[47] L. Patel,[19] M. Patel,[27] J.-C. Peng,[24] D. V. Perepelitsa,[7,13,14] G. D. N. Perera,[47] D. Yu. Peressounko,[33] J. Perry,[27] R. Petti,[7,59] C. Pinkenburg,[7] R. Pinson,[1] R. P. Pisani,[7] M. L. Purschke,[7] J. Rak,[29] B. J. Ramson,[41] I. Ravinovich,[64] K. F. Read,[49,60] D. Reynolds,[58] V. Riabov,[45,52] Y. Riabov,[52,56] T. Rinn,[27] N. Riveli,[48] D. Roach,[63] S. D. Rolnick,[8] M. Rosati,[27] Z. Rowan,[5] J. G. Rubin,[41] B. Sahlmueller,[59] N. Saito,[31] T. Sakaguchi,[7] H. Sako,[28] V. Samsonov,[45,52] M. Sarsour,[19] S. Sato,[28] S. Sawada,[31] B. Schaefer,[63] B. K. Schmoll,[60] K. Sedgwick,[8] J. Seele,[54] R. Seidl,[53,54] A. Sen,[27,60] R. Seto,[8] P. Sett,[4] A. Sexton,[39] D. Sharma,[59] I. Shein,[23] T.-A. Shibata,[53,61] K. Shigaki,[21] M. Shimomura,[27,44] P. Shukla,[4] A. Sickles,[7,24] C. L. Silva,[37] D. Silvermyr,[38,49] B. K. Singh,[3] C. P. Singh,[3] V. Singh,[3] M. Slunečka,[9] M. Snowball,[37] R. A. Soltz,[36] W. E. Sondheim,[37] S. P. Sorensen,[60] I. V. Sourikova,[7] P. W. Stankus,[49] M. Stepanov,[40,*] S. P. Stoll,[7] T. Sugitate,[21] A. Sukhanov,[7] T. Sumita,[53] J. Sun,[59] J. Sziklai,[65] A. Takahara,[12] A. Taketani,[53,54] K. Tanida,[54,57] M. J. Tannenbaum,[7] S. Tarafdar,[63,64] A. Taranenko,[45,58] R. Tieulent,[19] A. Timilsina,[27] T. Todoroki,[53,62] M. Tomášek,[15] H. Torii,[12] C. L. Towell,[1] M. Towell,[1] R. Towell,[1] R. S. Towell,[1] I. Tserruya,[64] H. W. van Hecke,[37] M. Vargyas,[16,65] J. Velkovska,[63] M. Virius,[15] V. Vrba,[15,26] E. Vznuzdaev,[52] X. R. Wang,[47,54] D. Watanabe,[21] Y. Watanabe,[53,54] Y. S. Watanabe,[12,31] F. Wei,[47] S. Whitaker,[27] A. S. White,[41] S. Wolin,[24] C. L. Woody,[7] M. Wysocki,[49] B. Xia,[48] L. Xue,[19] S. Yalcin,[59] Y. L. Yamaguchi,[12,59] A. Yanovich,[23] J. H. Yoo,[32] I. Yoon,[57] I. Younus,[35] H. Yu,[47,51] I. E. Yushmanov,[33] W. A. Zajc,[14] A. Zelenski,[6] S. Zhou,[11] and L. Zou[8]

(PHENIX Collaboration)

[1]*Abilene Christian University, Abilene, Texas 79699, USA*
[2]*Department of Physics, Augustana University, Sioux Falls, South Dakota 57197, USA*
[3]*Department of Physics, Banaras Hindu University, Varanasi 221005, India*
[4]*Bhabha Atomic Research Centre, Bombay 400 085, India*
[5]*Baruch College, City University of New York, New York, New York 10010, USA*
[6]*Collider-Accelerator Department, Brookhaven National Laboratory, Upton, New York 11973-5000, USA*
[7]*Physics Department, Brookhaven National Laboratory, Upton, New York 11973-5000, USA*
[8]*University of California-Riverside, Riverside, California 92521, USA*
[9]*Charles University, Ovocný trh 5, Praha 1, 116 36 Prague, Czech Republic*

[10]*Chonbuk National University, Jeonju 561-756, Korea*
[11]*Science and Technology on Nuclear Data Laboratory, China Institute of Atomic Energy, Beijing 102413, People's Republic of China*
[12]*Center for Nuclear Study, Graduate School of Science, University of Tokyo, 7-3-1 Hongo, Bunkyo, Tokyo 113-0033, Japan*
[13]*University of Colorado, Boulder, Colorado 80309, USA*
[14]*Columbia University, New York, New York 10027, USA, and Nevis Laboratories, Irvington, New York 10533, USA*
[15]*Czech Technical University, Zikova 4, 166 36 Prague 6, Czech Republic*
[16]*ELTE, Eötvös Loránd University, H-1117 Budapest, Pázmány P. s. 1/A, Hungary*
[17]*Ewha Womans University, Seoul 120-750, Korea*
[18]*Florida State University, Tallahassee, Florida 32306, USA*
[19]*Georgia State University, Atlanta, Georgia 30303, USA*
[20]*Hanyang University, Seoul 133-792, Korea*
[21]*Hiroshima University, Kagamiyama, Higashi-Hiroshima 739-8526, Japan*
[22]*Department of Physics and Astronomy, Howard University, Washington, DC 20059, USA*
[23]*IHEP Protvino, State Research Center of Russian Federation, Institute for High Energy Physics, Protvino 142281, Russia*
[24]*University of Illinois at Urbana-Champaign, Urbana, Illinois 61801, USA*
[25]*Institute for Nuclear Research of the Russian Academy of Sciences, Prospekt 60-letiya Oktyabrya 7a, Moscow 117312, Russia*
[26]*Institute of Physics, Academy of Sciences of the Czech Republic, Na Slovance 2, 182 21 Prague 8, Czech Republic*
[27]*Iowa State University, Ames, Iowa 50011, USA*
[28]*Advanced Science Research Center, Japan Atomic Energy Agency, 2-4 Shirakata Shirane, Tokai-mura, Naka-gun, Ibaraki-ken 319-1195, Japan*
[29]*Helsinki Institute of Physics and University of Jyväskylä, P.O. Box 35, FI-40014 Jyväskylä, Finland*
[30]*Károly Róberts University College, H-3200 Gyöngyös, Mátrai út 36, Hungary*
[31]*KEK, High Energy Accelerator Research Organization, Tsukuba, Ibaraki 305-0801, Japan*
[32]*Korea University, Seoul 136-701, Korea*
[33]*National Research Center "Kurchatov Institute", Moscow 123098, Russia*
[34]*Kyoto University, Kyoto 606-8502, Japan*
[35]*Physics Department, Lahore University of Management Sciences, Lahore 54792, Pakistan*
[36]*Lawrence Livermore National Laboratory, Livermore, California 94550, USA*
[37]*Los Alamos National Laboratory, Los Alamos, New Mexico 87545, USA*
[38]*Department of Physics, Lund University, Box 118, SE-221 00 Lund, Sweden*
[39]*University of Maryland, College Park, Maryland 20742, USA*
[40]*Department of Physics, University of Massachusetts, Amherst, Massachusetts 01003-9337, USA*
[41]*Department of Physics, University of Michigan, Ann Arbor, Michigan 48109-1040, USA*
[42]*Muhlenberg College, Allentown, Pennsylvania 18104-5586, USA*
[43]*Myongji University, Yongin, Kyonggido 449-728, Korea*
[44]*Nara Women's University, Kita-uoya Nishi-machi Nara 630-8506, Japan*
[45]*National Research Nuclear University, MEPhI, Moscow Engineering Physics Institute, Moscow 115409, Russia*
[46]*University of New Mexico, Albuquerque, New Mexico 87131, USA*
[47]*New Mexico State University, Las Cruces, New Mexico 88003, USA*
[48]*Department of Physics and Astronomy, Ohio University, Athens, Ohio 45701, USA*
[49]*Oak Ridge National Laboratory, Oak Ridge, Tennessee 37831, USA*
[50]*IPN-Orsay, Université Paris-Sud, CNRS/IN2P3, Université Paris-Saclay, BP1, F-91406 Orsay, France*
[51]*Peking University, Beijing 100871, People's Republic of China*
[52]*PNPI, Petersburg Nuclear Physics Institute, Gatchina, Leningrad region 188300, Russia*
[53]*RIKEN Nishina Center for Accelerator-Based Science, Wako, Saitama 351-0198, Japan*
[54]*RIKEN BNL Research Center, Brookhaven National Laboratory, Upton, New York 11973-5000, USA*
[55]*Physics Department, Rikkyo University, 3-34-1 Nishi-Ikebukuro, Toshima, Tokyo 171-8501, Japan*
[56]*Saint Petersburg State Polytechnic University, St. Petersburg, 195251, Russia*
[57]*Department of Physics and Astronomy, Seoul National University, Seoul 151-742, Korea*
[58]*Chemistry Department, Stony Brook University, SUNY, Stony Brook, New York 11794-3400, USA*
[59]*Department of Physics and Astronomy, Stony Brook University, SUNY, Stony Brook, New York 11794-3800, USA*
[60]*University of Tennessee, Knoxville, Tennessee 37996, USA*

[61]Department of Physics, Tokyo Institute of Technology, Oh-okayama, Meguro, Tokyo 152-8551, Japan
[62]Center for Integrated Research in Fundamental Science and Engineering, University of Tsukuba, Tsukuba, Ibaraki 305, Japan
[63]Vanderbilt University, Nashville, Tennessee 37235, USA
[64]Weizmann Institute, Rehovot 76100, Israel
[65]Institute for Particle and Nuclear Physics, Wigner Research Centre for Physics, Hungarian Academy of Sciences (Wigner RCP, RMKI) H-1525 Budapest 114, P.O. Box 49, Budapest, Hungary
[66]Yonsei University, IPAP, Seoul 120-749, Korea
[67]University of Zagreb, Faculty of Science, Department of Physics, Bijenička 32, HR-10002 Zagreb, Croatia
(Received 19 August 2016; published 29 December 2016)

We report the double-helicity asymmetry, $A_{LL}^{J/\psi}$, in inclusive J/ψ production at forward rapidity as a function of transverse momentum p_T and rapidity $|y|$. The data analyzed were taken during $\sqrt{s} = 510$ GeV longitudinally polarized $p + p$ collisions at the Relativistic Heavy Ion Collider in the 2013 run using the PHENIX detector. At this collision energy, J/ψ particles are predominantly produced through gluon-gluon scatterings, thus $A_{LL}^{J/\psi}$ is sensitive to the gluon polarization inside the proton. We measured $A_{LL}^{J/\psi}$ by detecting the decay daughter muon pairs $\mu^+\mu^-$ within the PHENIX muon spectrometers in the rapidity range $1.2 < |y| < 2.2$. In this kinematic range, we measured the $A_{LL}^{J/\psi}$ to be 0.012 ± 0.010 (stat) ± 0.003 (syst). The $A_{LL}^{J/\psi}$ can be expressed to be proportional to the product of the gluon polarization distributions at two distinct ranges of Bjorken x: one at moderate range $x \approx 5 \times 10^{-2}$ where recent data of jet and π^0 double helicity spin asymmetries have shown evidence for significant gluon polarization, and the other one covering the poorly known small-x region $x \approx 2 \times 10^{-3}$. Thus our new results could be used to further constrain the gluon polarization for $x < 5 \times 10^{-2}$.

DOI: 10.1103/PhysRevD.94.112008

I. INTRODUCTION

Understanding the proton spin structure in terms of quark and gluon degrees of freedom is one of the key open questions in the field of hadron physics. The total angular momentum of the proton may be decomposed into quark and gluon contributions in several different frameworks [1–6]. For example, in the infinite momentum frame, the contributions to the proton spin can be classified according to the Manohar-Jaffe sum rule [1,7,8]:

$$S_p = \frac{1}{2} = \frac{1}{2}\Delta\Sigma + \Delta G + L_q + L_g. \quad (1)$$

Here, $1/2\ \Delta\Sigma$ represents the contribution from quark helicity distributions (quark polarization projected onto the proton momentum direction); similarly, ΔG represents the contribution from gluon helicity distributions; L_q and L_g represent the contributions from orbital angular momenta of quarks and gluons respectively. The Manohar-Jaffe scheme has been widely used to directly compare theoretical expectations with experimental data in the infinite momentum frame for quark and gluon polarization contributions; however, the direct connection between orbital angular momentum and any corresponding experimental observable is still under debate [3,6].

The polarized parton distribution functions have been studied extensively at the European Laboratory for Particle Physics, the Stanford Linear Accelerator, the Deutsches Elektronen-Synchrotron, the Thomas Jefferson National Accelerator Facility and the Relativistic Heavy Ion Collider (RHIC) for decades. The most-recent-global quantum-chromodynamics (QCD) fits [9–14] based on these experimental data indicate that the quark polarization only accounts for about 30% of the proton spin. The remaining spin must come from the contributions from gluon polarization and from the orbital angular momentum of quarks and gluons. To resolve this "spin puzzle," it is critical to understand the contribution from gluon polarization [15–19].

Many hard-scale processes in $p + p$ collisions at RHIC energies are dominated by gluon-gluon and quark-gluon interactions; the corresponding spin observables are therefore sensitive to the gluon polarization. The latest global fits (DSSV [20], NNPDFpol [14], etc.) incorporating the RHIC 2009 inclusive jet [21] and π^0 [22] spin asymmetry data at midrapidity show the first experimental evidence of sizable gluon polarization at moderate Bjorken x in the range $0.05 \leq x \leq 0.2$. With higher statistics, a recent PHENIX $A_{LL}^{\pi^0}$ measurement [23] extended the small x reach down to

*Deceased.
†PHENIX Spokesperson.
akiba@bnl.gov

1×10^{-2} for the polarized gluon distribution. However, in the smaller-x region, $x < 1 \times 10^{-2}$, where gluons dominate, the gluon polarization remains poorly constrained.

The measurement of the double-helicity asymmetry in the production of J/ψ particles at forward rapidity can provide access to the gluon polarization in a smaller x region, $x \sim 2 \times 10^{-3}$. In $p+p$ collisions at RHIC energies, J/ψ particles are predominantly produced via gluon-gluon scatterings [24]. Therefore, at leading order, the asymmetry of J/ψ production can be expressed as

$$A_{LL}^{J/\psi} = \frac{\Delta\sigma}{\sigma} = \frac{\sigma^{++} - \sigma^{+-}}{\sigma^{++} + \sigma^{+-}} \tag{2}$$

$$\approx \frac{\Delta g(x_1)}{g(x_1)} \otimes \frac{\Delta g(x_2)}{g(x_2)} \otimes \hat{a}_{LL}^{gg \to J/\psi + X}, \tag{3}$$

where $A_{LL}^{J/\psi}$ is the J/ψ double-helicity asymmetry defined by the ratio of the polarized and unpolarized J/ψ cross sections ($\Delta\sigma$ and σ); "++" and "+−" denote the same and opposite helicity $p+p$ collisions; $\Delta g(x)$ and $g(x)$ are the polarized and unpolarized gluon parton distribution functions; and $\hat{a}_{LL}^{gg \to J/\psi + X}$ is the partonic double-helicity asymmetry for the process of $g + g \to J/\psi + X$. Due to the large charm quark mass, perturbative QCD is expected to work for calculations of the J/ψ and other charmonia production cross sections in high energy deep inelastic scattering and $p+p$ collisions. The production mechanisms of charmonia have been studied extensively for decades, and several theoretical approaches, including nonrelativistic QCD (NRQCD), have been developed to describe various experimental observations [25]. In high energy $p+p$ collisions, the individual partonic double-helicity asymmetry $\hat{a}_{LL}^{gg \to J/\psi + X}$ has been calculated in perturbative QCD for both color-singlet and color-octet mechanisms in the NRQCD framework, and used to calculate the inclusive $A_{LL}^{J/\psi}$ [24,26–28].

By detecting the J/ψ at forward rapidity, we sample participating gluons from two distinct ranges of Bjorken x. Quantitatively, we used a PYTHIA [29] (PYTHIA 6.4 tuned for RHIC energies) simulation at leading order to estimate the gluon x-distribution sampled in J/ψ production within the PHENIX muon arm acceptance. The simulation (Fig. 1) illustrates that for the $g + g \to J/\psi + X$ process in the forward rapidity of the PHENIX muon arm acceptance, the two gluons come from two very distinct x regions, with one gluon in the intermediate x range ($3 \times 10^{-2} - 2 \times 10^{-1}$) and the other gluon in the small x range ($1 \times 10^{-3} - 5 \times 10^{-3}$).

Several sources contribute to the inclusive J/ψ production, including decays from heavier states containing charm and/or bottom quarks. Previous studies in PHENIX [30] at midrapidity indicate that the excited states χ_c and ψ' contribute a sizable (30%–40%) portion of the inclusive

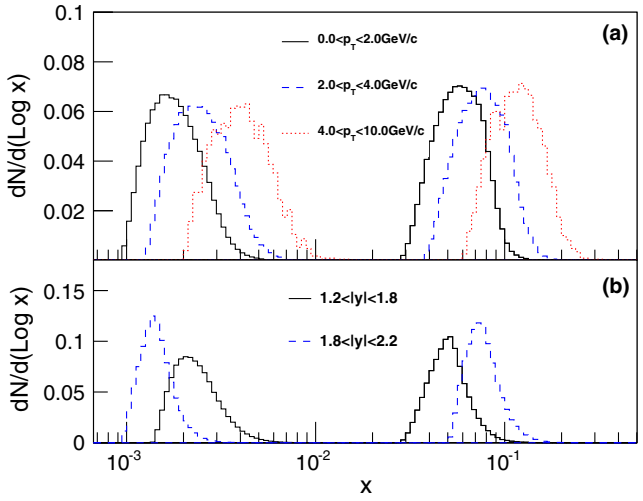

FIG. 1. Bjorken x distribution of gluons in the $gg \to J/\psi + X \to \mu^+\mu^- + X$ process from a PYTHIA simulation with J/ψ generated within $1.2 < |y| < 2.2$ and the decayed muon within $1.2 < |\eta| < 2.4$ for the north arm and $1.2 < |\eta| < 2.2$ for the south arm. The top panel shows the p_T binning and the bottom panel shows the $|y|$ binning. All the distributions are arbitrarily normalized to have unit area.

J/ψ production cross section. The $B \to J/\psi + X$ contribution is only important in the high $p_T > 10$ GeV region, and it is estimated to be small, less than 10% [31], in our kinematics at forward rapidity.

In the following, we present the measurement of the double-helicity asymmetry in inclusive J/ψ production in longitudinally polarized $p+p$ collisions at $\sqrt{s} = 510$ GeV. The data used for the study were collected by the PHENIX experiment [32] during the 2013 run; the sampled integrated luminosity was about 150 pb^{-1} for this analysis.

II. EXPERIMENT SETUP AND DATA ANALYSIS

The J/ψ mesons were observed in the dimuon $\mu^+\mu^-$ decay channel using the two PHENIX forward muon spectrometers. Each spectrometer arm has full azimuthal coverage and spans the pseudorapidity range $1.2 < |\eta| < 2.4$ for the north arm and $1.2 < |\eta| < 2.2$ for the south arm. The major detector subsystems involved in this analysis were the muon trackers (MuTr) and the muon identifiers (MuID) [33], the beam-beam counters (BBC), the zero-degree calorimeters (ZDC) [34], and the forward-silicon-vertex detectors (FVTX) [35].

The muon momentum was measured by the MuTr, a system based on three layers of cathode-strip tracking chambers in a radial-field magnet. The MuID comprises five layers of Iarocci tubes interleaved with 10 or 20 cm thick steel absorbers. The MuID absorbers, together with the central magnet absorbers (a combination of copper, iron and stainless steel, approximately 100 cm thick), were used to suppress light hadron backgrounds (pions and kaons) while allowing high energy muons to pass through. The

probability of a high energy hadron ($p > 3$ GeV) generated from the interaction point (IP) passing through all the absorbers and getting mistagged as a muon is less than 3% [33] in $p + p$ collisions.

The BBC comprises two quartz Čerenkov modules located on opposite sides of the IP at $z = \pm 144$ cm, where z is the distance in the beam direction from the IP, and covering a pseudorapidity range of $3.1 < |\eta| < 3.9$ and full azimuth. The BBC system measures the collision vertex position along the beam direction via a time-of-flight method and also serves as one of the luminosity detectors.

Muon candidate events were selected using a BBC-based minimum-bias collision trigger in coincidence with a MuID track-based trigger. The MuID triggers were defined by various combinations of hits in several layers of the MuID projecting to the IP. A "deep" MuID track requires at least one hit in the last two layers of the MuID detector and at least two hits in other layers. In the PHENIX 2013 run detector shielding configuration, a minimum momentum of ~ 3 GeV/c was needed for muons to reach the last layer of the MuID. The data set we used was selected by the "2-Deep Muon Trigger" which required at least two MuID deep tracks in the same muon arm in a $p + p$ collision event. A more detailed description of the 2-Deep Muon Trigger is found in Ref. [36].

The ZDC detector comprises two hadron calorimeter arms at $|z| = 18$ m. It covers a pseudorapidity range of $|\eta| > 6$. In this analysis, the ZDC served as a second luminosity detector for systematic studies.

The FVTX detector is composed of two end caps upstream of the MuTr [35]. By searching for common origin points of the detected tracks, the FVTX is capable of reconstructing primary collision vertices in the z range used in this measurement. The FVTX vertex resolution along the beam line direction is at the one millimeter level, which is much more precise than the vertex resolution of the BBC detector. In this analysis, the FVTX vertices were used when available to improve the mass resolution of the dimuon pairs.

For optimal use of the muon spectrometers, the collision vertex reconstructed by the BBC was required to be within ± 30 cm of the IP along the beam direction. Each muon track candidate was required to have a longitudinal momentum $p_z < 100$ GeV/c and transverse momentum $p_T < 10$ GeV/c. The distance between the projected MuTr track and MuID track position at the first layer of the MuID plane was required to be less than 15 cm, and the projected opening angle between the MuTr track and the MuID track less than 10 degrees. Similar MuTr and MuID track matching cuts were used in Ref. [36]. A fit to the common vertex of the two candidate tracks near the IP was performed and was required to have a $\chi^2 < 20$ for 4 degrees of freedom. The black circle data points in Fig. 2 show the invariant mass distribution of the unlike-sign dimuon pairs after event and track quality selections.

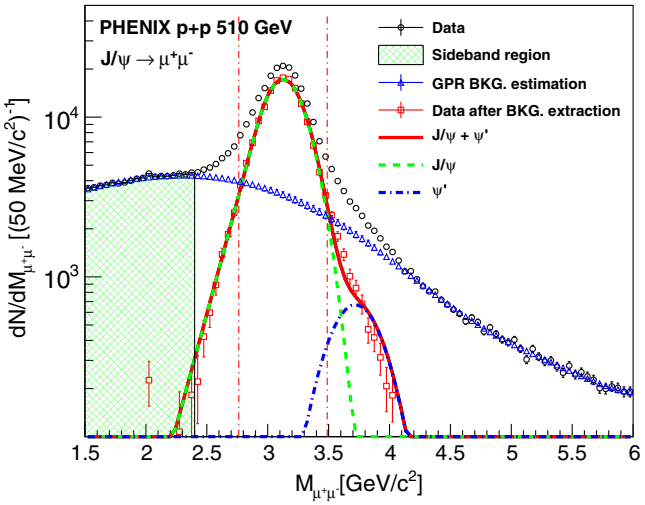

FIG. 2. Dimuon invariant mass spectrum and the GPR fitting for the background fraction f_{Bkg} extraction. The black circles are the PHENIX unlike-sign dimuon data after event and track selection. The blue triangles are the GPR background estimation. The red boxes are the data remaining after subtraction of the background. The green dashed line represents the J/ψ shape; the blue dot-dashed line represents the ψ' shape; and the red solid line the summation of J/ψ and ψ'. The green shaded region indicates the sideband area used for the calculation of A_{LL}^{Bkg} in Eq. (8). The data in the region between the two red vertical lines are the data used to calculate A_{LL}^{Incl} in Eq. (8).

At RHIC, the clockwise ("Blue") and counterclockwise ("Yellow") circulating beams collide at several fixed IPs, the PHENIX detector being one of them. During the 2013 longitudinally polarized $p + p$ run, up to 111 radio-frequency bunches in each beam were filled with protons. Protons in each bunch were configured to have positive or negative helicity, denoted as "+" or "−." Thus collisions at the PHENIX IP can be categorized into two helicity combinations: same helicity (denoted as $++$) and opposite helicity (denoted as $+-$) collisions. For parity-conserving QCD processes, the production cross sections obey the relations $\sigma^{++} = \sigma^{--}$ and $\sigma^{+-} = \sigma^{-+}$. Experimentally, the double helicity asymmetry is defined as

$$A_{LL} = \frac{\sigma^{++} - \sigma^{+-}}{\sigma^{++} + \sigma^{+-}} = \frac{1}{P_B P_Y} \frac{N^{++} - R \cdot N^{+-}}{N^{++} + R \cdot N^{+-}}, \quad (4)$$

where P_B (P_Y) is the beam polarization for the Blue (Yellow) beam, σ^{++} (σ^{+-}) is the cross section for same (opposite) helicity collisions, and N^{++} (N^{+-}) is the produced dimuon yield for same (opposite) helicity collisions. R is the relative luminosity between helicity states and is defined as

$$R = \frac{L^{++}}{L^{+-}}, \quad (5)$$

where $L^{++}(L^{+-})$ is the luminosity measured by the BBC detectors in $++(+-)$ helicity state collisions. The averaged polarizations for the data used in this analysis were

$$P_B = 0.55 \pm 0.02(\text{syst}), \tag{6}$$

$$P_Y = 0.56 \pm 0.02(\text{syst}). \tag{7}$$

For each "fill" (a unit of the operation period of the accelerator, typically several hours) of the rings, the helicity pattern was designed to provide almost equal numbers of collisions in the $++$, $+-$, $-+$, and $--$ helicity configurations. In this way, slow changes in detector acceptance and efficiency were eliminated from the asymmetry determination in Eq. (4).

As shown in Fig. 2, there is a small amount (∼15%) of dimuon background underneath the J/ψ signal peak in the dimuon invariant mass distribution; the background events may have a different asymmetry from that of J/ψ events. To correct for this, we estimated the background asymmetry using the "sideband" in the invariant mass region (1.5–2.4 GeV/c^2), the green shaded region in Fig. 2. Consistent with Ref. [36], this sideband was located below the J/ψ peak in invariant mass; a sideband that was higher in invariant mass would need to be placed further away from the J/ψ to avoid the ψ' and would have had negligible statistical significance. For the final J/ψ double-helicity asymmetry, we subtracted the background contributions:

$$A_{LL}^{J/\psi} = \frac{A_{LL}^{\text{Incl}} - f_{\text{Bkg}} \cdot A_{LL}^{\text{Bkg}}}{1 - f_{\text{Bkg}}}, \tag{8}$$

where A_{LL} values on the right-hand side were calculated using Eq. (4). The asymmetry A_{LL}^{Incl} is for inclusive unlike-charge dimuon pairs in the invariant mass region $\pm 2\sigma$ around the J/ψ mass peak mean value (σ is the mass resolution of the detector), and A_{LL}^{Bkg} is the asymmetry for a sideband of unlike-charge dimuon pairs. In this analysis, the measured A_{LL}^{Bkg} was $-0.002 \pm 0.012(\text{stat})$ for the p_T range $0 < p_T < 10$ GeV. The background fraction f_{Bkg} is defined as

$$f_{\text{Bkg}} = \frac{N_{\text{Bkg}}}{N_{\text{Incl}}}, \tag{9}$$

where N_{Bkg} is the number of estimated non-J/ψ dimuon pairs in the $\pm 2\sigma$ range around the J/ψ peak, and N_{Incl} is the total number of unlike-charge dimuon pairs in the same mass range. For the background under the J/ψ mass peak, a Gaussian process regression (GPR) [37–41] approach was used to determine the background distribution. Two training zones, on either side of the J/ψ peak, were defined for this GPR approach: 1.5–2.2 GeV/c^2 and 4.3–6.0 GeV/c^2. These two training zones were used only for the estimation of background yield, not the background asymmetry. The $J/\psi 2\sigma$ mass window was defined by fitting the data after the GPR background subtraction. In the fitting, the J/ψ invariant mass peak shape was described by a Crystal Ball distribution [42], and for simplicity the low statistics ψ' peak was fit with a Gaussian distribution with mass resolution evaluated from Monte Carlo simulation.

TABLE I. Background fraction f_{Bkg} for each arm and each p_T or $|y|$ bin using the corresponding $J/\psi 2\sigma$ mass window for that bin. The systematic uncertainty is 0.05 (absolute value) for all the bins; see discussion in the text.

p_T or $\lvert y\rvert$ range	$f_{\text{Bkg}} \pm \Delta f_{\text{Bkg}}(\text{stat})$
$0 < p_T < 2$ GeV/c	0.26 ± 0.01
$2 < p_T < 4$ GeV/c	0.17 ± 0.01
$4 < p_T < 10$ GeV/c	0.18 ± 0.01
$1.2 < \lvert y\rvert < 1.8$	0.25 ± 0.02
$1.8 < \lvert y\rvert < 2.2$	0.30 ± 0.02

In this analysis, we measured the asymmetry separately for the two muon arms. The results were then cross-checked for consistency and combined to produce the final physics double-helicity asymmetry.

To further study the p_T or $|y|$ dependence of the asymmetry, the data were divided into three p_T bins (0–2, 2–4, and 4–10 GeV/c) or two $|y|$ bins (1.2–1.8, 1.8–2.2). $A_{LL}^{J/\psi}$ was extracted for each of the bins following the procedure described above; the corresponding background fraction f_{Bkg} was extracted and is listed in Table I.

The statistical uncertainties for $A_{LL}^{J/\psi}$ ($\Delta A_{LL}^{J/\psi}$) were calculated via Eq. (10):

$$\Delta A_{LL}^{J/\psi} = \frac{\sqrt{(\Delta A_{LL}^{\text{Incl}})^2 + (f_{\text{Bkg}} \cdot \Delta A_{LL}^{\text{Bkg}})^2}}{1 - f_{\text{Bkg}}}, \tag{10}$$

where $\Delta A_{LL}^{\text{Incl}}$ and $\Delta A_{LL}^{\text{Bkg}}$ represent the statistical uncertainty of the A_{LL}^{Incl} and A_{LL}^{Bkg} respectively. The statistical uncertainty of f_{Bkg} is combined with its systematic uncertainty from the extraction method and considered as one of the systematic uncertainties which is discussed in the next section.

III. SYSTEMATIC UNCERTAINTY

There are two types of systematic uncertainties involved in this analysis: Type A are uncorrelated point-to-point uncertainties for each p_T or $|y|$ bin, and type B are correlated point-to-point uncertainties.

One important type A systematic uncertainty comes from the determination of the background fraction under the J/ψ mass peak. To test the possible bias of the background fraction f_{Bkg} extracted from the GPR procedure, we compared to the method that was used in [36]

which used a third order polynomial to describe the background. The two methods differed at most by 0.05 (absolute value); we took that as the systematic uncertainty for the background fraction f_{Bkg}.

Another type A systematic uncertainty is from the determination of background asymmetry under the J/ψ mass peak. Because the low mass side band was used to estimate the background spin asymmetry under the J/ψ mass peak, we need to estimate the bias introduced by this approximation. We studied the mass dependence of the background asymmetry by dividing the sideband into two mass bins, 1.5–2.0 GeV/c^2 and 2.0–2.4 GeV/c^2. We found no obvious mass dependence beyond expected statistical fluctuation. Thus we concluded that this systematic uncertainty related to the mass dependence of the background asymmetry is small compared with the statistical uncertainty of the sideband dimuon asymmetry [$\Delta A_{LL}^{\mathrm{Bkg}}$ in Eq. (10)] and is not counted as additional uncertainty for this analysis.

The last type A systematic uncertainty comes from the variation of detector efficiency within a data group in which the asymmetry is calculated. For the purpose of getting sufficient statistics in the asymmetry calculations using Eq. (4) discussed above, we collected individual PHENIX runs into larger groups, each of which corresponds to a time period of up to 1.5 hour of continuous data acquisition. However, the detector efficiency may vary between runs in each group, and that could lead to a biased result. The muon reconstruction efficiency has a dependence on the luminosity and event vertex distribution and it could also change over time. To study this systematically, three grouping methods were applied and compared with each other: (1) runs with similar luminosity and event vertex distribution; (2) runs within a RHIC fill to minimize the time spreading of each group; (3) all the runs into one group. We chose method (1) results to calculate the mean value of our results. The systematic uncertainty from the grouping method was set to the maximum variation extracted from these three approaches. Type A systematic uncertainties for all p_T or $|y|$ bins are summarized in Table II.

The systematic uncertainty in the determination of the relative luminosity is of type B. The luminosities $L^{++,+-}$, and therefore also the relative luminosity R used in Eq. (4), were measured by the BBC trigger counts with a vertex cut of ± 30 cm along the beam line. To test if the BBC count rate contains an unmeasured physics asymmetry, we used another luminosity detector, the ZDC, and computed the double-helicity asymmetry of the ZDC/BBC luminosity ratio:

$$A_{LL}^{\mathrm{ZDC/BBC}} = \frac{1}{P_B P_Y} \frac{\frac{N_{\mathrm{ZDC}}^{++}}{N_{\mathrm{BBC}}^{++}} - \frac{N_{\mathrm{ZDC}}^{+-}}{N_{\mathrm{BBC}}^{+-}}}{\frac{N_{\mathrm{ZDC}}^{++}}{N_{\mathrm{BBC}}^{++}} + \frac{N_{\mathrm{ZDC}}^{+-}}{N_{\mathrm{BBC}}^{+-}}}, \tag{11}$$

where N_{ZDC} (N_{BBC}) is the coincidence counts measured by the ZDC (BBC), which is proportional to the beam luminosity. During the 2013 PHENIX 510 GeV $p+p$ run, due to high beam intensity, approximately 30% of bunch crossings contain more than one $p+p$ binary collision. However, neither the BBC nor the ZDC can separate these multiple collisions. Therefore, multiple collisions are counted as one $p+p$ collision and this affects the determination of the relative luminosity. A statistical pileup correction was performed to remove the bias of the (relative) luminosity measurement caused by multiple collisions, identical to the correction performed in Ref. [23]. We took the asymmetry $A_{LL}^{\mathrm{ZDC/BBC}}$ plus its statistical uncertainty as a systematic uncertainty for the relative luminosity R. After pileup corrections the systematic uncertainty from relative luminosity was determined to be 4×10^{-4}.

Another source of systematic uncertainty (type B) comes from the measurement of the average beam polarizations, P_B and P_Y. The uncertainty of the product $P_B P_Y$ used in Eq. (4) leads to an overall scale uncertainty of the A_{LL} measurements. For the RHIC 2013 data set, this uncertainty was evaluated to be $6.5\% \times A_{LL}$. The residual transverse polarization component in the interaction region is very small (the longitudinal polarization component is $> 99.8\%$) and the associated effect on the overall scale is smaller than $10^{-3} \times A_{LL}$ and is thus negligible for this analysis.

A technique called "bunch shuffling" [22] was applied to test for additional RHIC bunch-to-bunch and fill-to-fill uncorrelated systematic uncertainties that may have been overlooked. The resulting $A_{LL}^{\mathrm{shuffle}}$ follows a Gaussian distribution with σ consistent with the statistical uncertainty of $A_{LL}^{J/\psi}$ obtained with real data. This test result indicates that all other uncorrelated bunch-to-bunch and fill-to-fill systematic uncertainties are much smaller than the statistical uncertainties.

TABLE II. Type A systematic uncertainties for each p_T or $|y|$ bin. $\Delta A_{LL}^{\mathrm{fit}}$ is the systematic uncertainty from background fraction determination. $\Delta A_{LL}^{\mathrm{run\ group}}$ is the systematic uncertainty from the run grouping method.

p_T or $\lvert y\rvert$ range	$\Delta A_{LL}^{\mathrm{fit}}$	$\Delta A_{LL}^{\mathrm{run\ group}}$
$0 < p_T < 2$ GeV/c	<0.001	0.003
$2 < p_T < 4$ GeV/c	0.001	0.004
$4 < p_T < 10$ GeV/c	0.003	0.009
$1.2 < \lvert y\rvert < 1.8$	0.005	0.004
$1.8 < \lvert y\rvert < 2.2$	0.002	0.002

IV. RESULTS AND SUMMARY

The final results for $J/\psi A_{LL}$ as a function of p_T and $|y|$ are summarized in Table III and in Fig. 3. The average $A_{LL}^{J/\psi}$ measured is 0.012 ± 0.010 (stat) ± 0.003 (syst).

TABLE III. $A_{LL}^{J/\psi}$ as a function of p_T or $|y|$. $N_{J/\psi}^{2\sigma}$ is the J/ψ counting within its 2σ mass window. The column of type A systematic uncertainties are a statistically weighted quadratic combination of the background fraction and run grouping uncertainties. ΔA_{LL} (relative luminosity) is the global systematic uncertainty from relative luminosity measurements. ΔA_{LL} (polarization) is the systematic uncertainty from the beam polarization measurement.

p_T (GeV/c) or $\|y\|$ bin	$\langle p_T\rangle$(GeV/c) or $\langle\|y\|\rangle$	$N_{J/\psi}^{2\sigma}$ ×10000	$A_{LL}^{J/\psi}$	ΔA_{LL} (stat)	ΔA_{LL} (Type A syst)	ΔA_{LL} (relative luminosity) (Type B syst)	ΔA_{LL} (polarization) (Type B syst)
$p_T \in$ (0–10)	$\langle p_T\rangle = 2.03$ GeV/c	15.9	0.012	0.010	0.003	0.0004	0.001
$\|y\| \in$ (1.2–2.2)	$\langle\|y\|\rangle = 1.71$						
$p_T \in$ (0–2)	1.12	8.8	0.003	0.014	0.003	0.0004	<0.001
$p_T \in$ (2–4)	2.79	5.6	0.007	0.016	0.004	0.0004	<0.001
$p_T \in$ (4–10)	5.25	1.7	0.057	0.029	0.010	0.0004	0.004
$\|y\| \in$ (1.2–1.8)	1.59	10.2	0.025	0.013	0.006	0.0004	0.002
$\|y\| \in$ (1.8–2.2)	1.94	4.9	0.001	0.019	0.003	0.0004	<0.001

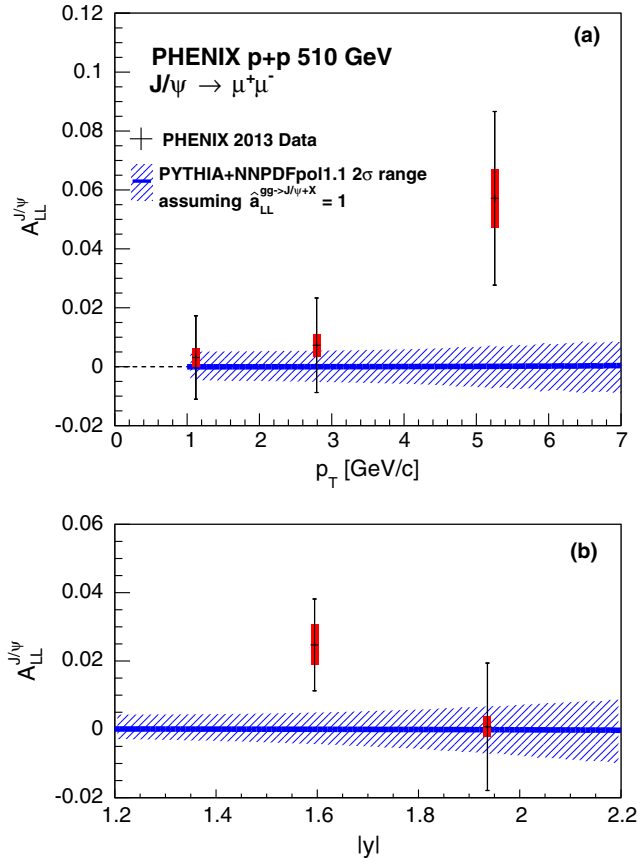

FIG. 3. $A_{LL}^{J/\psi}$ as a function of p_T (top panel) and $|y|$ (bottom panel). The black error bars show the statistical uncertainty. The red boxes show only the type A systematic uncertainties. There are additionally a 4×10^{-4} global systematic uncertainty from the relative luminosity determination and a 6.5% global scaling systematic uncertainty from the polarization magnitude determination for all p_T or $|y|$ bins. The blue curve with shaded band is our $A_{LL}^{J/\psi}$ estimation using PYTHIA6 [29] simulation with NNPDFpol1.1 data sets under the assumption of $\hat{a}_{LL}^{gg\to J/\psi+X} = 1$. The solid blue curve is the central value and the blue shaded band is the $\pm 2\sigma$ uncertainty range. See details in the text.

There were several NRQCD calculations of the $A_{LL}^{J/\psi}$ for RHIC energies $\sqrt{s} = 200$ GeV and $\sqrt{s} = 500$ GeV [26] but with the Gehrmann-Stirling and other polarized parton distribution functions [43] produced in the 1990s. Our knowledge of quark and gluon polarizations has been significantly improved over the past 10 years [14,20]. To compare our results with the current understanding of the gluon polarization, we have calculated the $A_{LL}^{J/\psi}$ in our kinematic range using a PYTHIA [29] simulation with NNPDFpol1.1 [14] and NNPDF3.0 [44] as the polarized and unpolarized PDF respectively. To separate the uncertainty from the J/ψ production mechanism, we have assumed $\hat{a}_{LL}^{gg\to J/\psi+X} = 1$, which is the leading order partonic asymmetry for open heavy quarks in the heavy mass limit at RHIC energies [24]. A 2σ uncertainty band was also calculated using the replica method as presented in Ref. [45]. The calculated asymmetry using these assumptions is shown in Fig. 3 together with the PHENIX data. The calculated asymmetry is consistent with our data within the statistical uncertainties.

A reweighting method that estimates the impact of a new data set on the PDFs without doing a new global fit was introduced by the NNPDF Collaboration [46]. Using this method we estimated the impact of our data on the gluon polarization based on NNPDFpol1.1 and under the assumption of $\hat{a}_{LL}^{gg\to J/\psi+X} = 1$. Figure 4 shows the gluon polarization before and after reweighting. In this reweighting, only the statistical uncertainty of our data was considered. Under this assumption, our data favors a more positive gluon polarization in the $x \sim 2 \times 10^{-3}$ region compared to the original NNPDFpol1.1.

In summary, the double-helicity asymmetries of inclusive J/ψ production have been measured with the PHENIX detector as a function of the J/ψ 's p_T and $|y|$, covering $0 < p_T < 10$ GeV and rapidity $1.2 < |y| < 2.2$. The $A_{LL}^{J/\psi}$ measurements offer a new way to access ΔG via heavy-quark production in $p + p$ collisions. They also serve as an important test of the universality of the helicity-dependent parton densities and QCD factorizations.

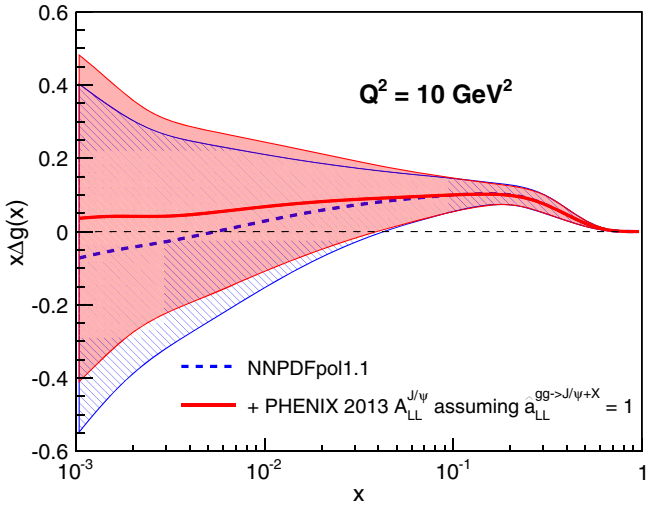

FIG. 4. Blue dashed line is gluon polarization in NNPDFpol1.1; uncertainty band for it was obtained from 100 replicas of NNPDFpol1.1 using the replica method in [45]. The red solid curve is the gluon polarization from NNPDFpol1.1 reweighted using 2013 PHENIX $J/\psi A_{LL}$ data under the assumption that $\hat{a}_{LL}^{gg\to J/\psi+X} = 1$.

ACKNOWLEDGMENTS

We thank the staff of the Collider-Accelerator and Physics Departments at Brookhaven National Laboratory and the staff of the other PHENIX participating institutions for their vital contributions. We also thank E. R. Nocera for helpful discussions on the reweighting using NNPDFpol1.1. We acknowledge support from the Office of Nuclear Physics in the Office of Science of the Department of Energy, the National Science Foundation, Abilene Christian University Research Council, Research Foundation of SUNY, and Dean of the College of Arts and Sciences, Vanderbilt University (U.S.A.), Ministry of Education, Culture, Sports, Science, and Technology and the Japan Society for the Promotion of Science (Japan), Conselho Nacional de Desenvolvimento Científico e Tecnológico and Fundação de Amparo à Pesquisa do Estado de São Paulo (Brazil), Natural Science Foundation of China (People's Republic of China), Croatian Science Foundation and Ministry of Science, Education, and Sports (Croatia), Ministry of Education, Youth and Sports (Czech Republic), Centre National de la Recherche Scientifique, Commissariat à l'Énergie Atomique, and Institut National de Physique Nucléaire et de Physique des Particules (France), Bundesministerium für Bildung und Forschung, Deutscher Akademischer Austausch Dienst, and Alexander von Humboldt Stiftung (Germany), National Science Fund, OTKA, Károly Róbert University College, and the Ch. Simonyi Fund (Hungary), Department of Atomic Energy and Department of Science and Technology (India), Israel Science Foundation (Israel), Basic Science Research Program through NRF of the Ministry of Education (Korea), Physics Department, Lahore University of Management Sciences (Pakistan), Ministry of Education and Science, Russian Academy of Sciences, Federal Agency of Atomic Energy (Russia), VR and Wallenberg Foundation (Sweden), the U.S. Civilian Research and Development Foundation for the Independent States of the Former Soviet Union, the Hungarian American Enterprise Scholarship Fund, and the U.S.-Israel Binational Science Foundation.

[1] R. L. Jaffe and A. Manohar, The G(1) problem: Fact and fantasy on the spin of the proton, Nucl. Phys. **B337**, 509 (1990).
[2] X.-D. Ji, Gauge-Invariant Decomposition of Nucleon Spin, Phys. Rev. Lett. **78**, 610 (1997).
[3] X.-S. Chen, W.-M. Sun, F. Wang, and T. Goldman, Proper identification of the gluon spin, Phys. Lett. B **700**, 21 (2011).
[4] Y. Hatta, Gluon polarization in the nucleon demystified, Phys. Rev. D **84**, 041701 (2011).
[5] X. Ji, J.-H. Zhang, and Y. Zhao, Physics of the Gluon-Helicity Contribution to Proton Spin, Phys. Rev. Lett. **111**, 112002 (2013).
[6] M. Wakamatsu, More on the relation between the two physically inequivalent decompositions of the nucleon spin and momentum, Phys. Rev. D **85**, 114039 (2012).
[7] X. Ji, J.-H. Zhang, and Y. Zhao, Justifying the naive partonic sum rule for proton spin, Phys. Lett. B **743**, 180 (2015).
[8] E. Leader, On the controversy concerning the definition of quark and gluon angular momentum, Phys. Rev. D **83**, 096012 (2011); Erratum, Phys. Rev. D **85**, 039905(E) (2012).
[9] D. de Florian, R. Sassot, M. Stratmann, and W. Vogelsang, Global Analysis of Helicity Parton Densities and Their Uncertainties, Phys. Rev. Lett. **101**, 072001 (2008).
[10] D. de Florian, R. Sassot, M. Stratmann, and W. Vogelsang, Extraction of spin-dependent parton densities and their uncertainties, Phys. Rev. D **80**, 034030 (2009).
[11] E. Leader, A. V. Sidorov, and D. B. Stamenov, Determination of polarized PDFs from a QCD analysis of inclusive and semi-inclusive deep inelastic scattering data, Phys. Rev. D **82**, 114018 (2010).
[12] J. Blumlein and H. Bottcher, QCD analysis of polarized deep inelastic scattering data, Nucl. Phys. **B841**, 205 (2010).
[13] M. Hirai and S. Kumano, Determination of gluon polarization from deep inelastic scattering and collider data, Nucl. Phys. **B813**, 106 (2009).

[14] E. R. Nocera, R. D. Ball, S. Forte, G. Ridolfi, and J. Rojo (NNPDF Collaboration), A first unbiased global determination of polarized PDFs and their uncertainties, Nucl. Phys. **B887**, 276 (2014).

[15] G. Altarelli and G. G. Ross, The anomalous gluon contribution to polarized leptoproduction, Phys. Lett. B **212**, 391 (1988).

[16] R. D. Carlitz, J. C. Collins, and A. H. Mueller, The role of the axial anomaly in measuring spin dependent parton distributions, Phys. Lett. B **214**, 229 (1988).

[17] J. Fischer, P. Kolár, and V. Kundrát, *Hadron Interactions: Proceedings of the International Symposium "Hadron Interactions - Theory and Phenomenology," Bechyne, Czechoslovakia* (Institute of physics, 1988).

[18] M. Anselmino, B. L. Ioffe, and E. Leader, On possible resolutions of the spin crisis in the parton model, Yad. Fiz. **49**, 214 (1989) [Sov. J. Nucl. Phys. **49**, 136 (1989)].

[19] T. Morii, S. Tanaka, and T. Yamanishi, Effects of the large gluon polarization on $xg_1^d(x)$ and J/ψ productions at polarized ep and pp collisions, Phys. Lett. B **322**, 253 (1994).

[20] D. de Florian, R. Sassot, M. Stratmann, and W. Vogelsang, Evidence for Polarization of Gluons in the Proton, Phys. Rev. Lett. **113**, 012001 (2014).

[21] L. Adamczyk *et al.* (STAR Collaboration), Precision Measurement of the Longitudinal Double-spin Asymmetry for Inclusive Jet Production in Polarized Proton Collisions at $\sqrt{s} = 200$ GeV, Phys. Rev. Lett. **115**, 092002 (2015).

[22] A. Adare *et al.* (PHENIX Collaboration), Inclusive double-helicity asymmetries in neutral-pion and eta-meson production in $\vec{p} + \vec{p}$ collisions at $\sqrt{s} = 200$ GeV, Phys. Rev. D **90**, 012007 (2014).

[23] A. Adare *et al.* (PHENIX Collaboration), Inclusive cross section and double-helicity asymmetry for π^0 production at midrapidity in $p + p$ collisions at $\sqrt{s} = 510$ GeV, Phys. Rev. D **93**, 011501 (2016).

[24] S. Gupta and P. Mathews, χ_1 and polarization asymmetries for quarkonia at high orders in nonrelativistic QCD, Phys. Rev. D **56**, 7341 (1997).

[25] J. P. Lansberg, J/ψ, ψ' and Υ production at hadron colliders: A review, Int. J. Mod. Phys. A **21**, 3857 (2006).

[26] A. Tkabladze and O. Teryaev, Double spin asymmetry of J/ψ production in polarized pp collisions at HERA-N, Phys. Rev. D **56**, 7331 (1997).

[27] M. Klasen, B. A. Kniehl, L. N. Mihaila, and M. Steinhauser, Charmonium production in polarized high-energy collisions, Phys. Rev. D **68**, 034017 (2003).

[28] Z. Yujie and M. Yanqing (private communication).

[29] T. Sjöstrand, S. Mrenna, and P. Skands, PYTHIA 6.4 physics and manual, J. High Energy Phys. 05 (2006) 026.

[30] A. Adare *et al.* (PHENIX Collaboration), Ground and excited charmonium state production in $p + p$ collisions at $\sqrt{s} = 200$ GeV, Phys. Rev. D **85**, 092004 (2012).

[31] S. Chatrchyan *et al.* (CMS Collaboration), Suppression of non-prompt J/ψ, prompt J/ψ, and $\Upsilon(1S)$ in PbPb collisions at $\sqrt{s_{NN}} = 2.76$ TeV, J. High Energy Phys. 05 (2012) 063.

[32] K. Adcox *et al.* (PHENIX Collaboration), PHENIX detector overview, Nucl. Instrum. Methods Phys. Res., Sect. A **499**, 469 (2003).

[33] H. Akikawa *et al.* (PHENIX Collaboration), PHENIX muon arms, Nucl. Instrum. Methods Phys. Res., Sect. A **499**, 537 (2003).

[34] C. Adler, A. Denisov, E. Garcia, M. J. Murray, H. Strobele, and S. N. White, The RHIC zero degree calorimeter, Nucl. Instrum. Methods Phys. Res., Sect. A **470**, 488 (2001).

[35] C. Aidala *et al.*, The PHENIX forward silicon vertex detector, Nucl. Instrum. Methods Phys. Res., Sect. A **755**, 44 (2014).

[36] A. Adare *et al.* (PHENIX Collaboration), Measurement of transverse single-spin asymmetries for J/ψ production in polarized $p + p$ collisions at $\sqrt{s} = 200$ GeV, Phys. Rev. D **82**, 112008 (2010); Erratum, Phys. Rev. D **86**, 099904(E) (2012).

[37] D. J. MacKay, *Information Theory, Inference and Learning Algorithms* (Cambridge University Press, Cambridge, 2003).

[38] C. E. Rasmussen and C. K. I. Williams, *Gaussian Processes for Machine Learning* (MIT Press, Cambridge, MA, 2006).

[39] S. L. Lauritzen, *Graphical Models* (Clarendon Press and Oxford University Press, Oxford, 1996).

[40] D. Barber, *Bayesian Reasoning and Machine Learning* (Cambridge University Press, Cambridge, 2012).

[41] A. Adare *et al.* (PHENIX Collaboration), Measurement of parity-violating spin asymmetries in $W^{\pm}$ production at midrapidity in longitudinally polarized $p + p$ collisions, Phys. Rev. D **93**, 051103 (2016).

[42] T. Skwarnicki, A study of the radiative CASCADE transitions between the Upsilon-Prime and Upsilon resonances, Ph.D. thesis, Institute of Nuclear Physics, Cracow, Poland, 1986.

[43] T. Gehrmann and W. J. Stirling, Polarized parton distributions in the nucleon, Phys. Rev. D **53**, 6100 (1996).

[44] R. D. Ball *et al.* (NNPDF Collaboration), Parton distributions for the LHC run II, J. High Energy Phys. 04 (2015) 040.

[45] J. Gao and P. Nadolsky, A meta-analysis of parton distribution functions, J. High Energy Phys. 07 (2014) 035.

[46] R. D. Ball, V. Bertone, F. Cerutti, L. Del Debbio, S. Forte, A. Guffanti, J. I. Latorre, J. Rojo, and M. Ubiali (NNPDF Collaboration), Reweighting NNPDFs: The W lepton asymmetry, Nucl. Phys. **B849**, 112 (2011); Erratum, Nucl. Phys. **855**, 927(E) (2012).